Journal of Control, Automation and Electrical Systems (2018) 29:480–488
https://doi.org/10.1007/s40313-018-0383-x

Evaluation of the Output Load Effect on a Piezoelectric Energy Harvester

M. A. J. Coelho[1] · **J. V. Flores**[1] · **V. J. Brusamarello**[1]

Received: 3 November 2017 / Revised: 18 January 2018 / Accepted: 28 March 2018 / Published online: 11 April 2018
© Brazilian Society for Automatics–SBA 2018

Abstract
This paper presents the study of a vibration energy harvesting system using piezoelectric generator coupled to a cantilever beam when subjected to output loads with different electrical characteristics. The proposed analysis is based on the system frequency response under two scenarios at the output of the piezoelectric energy harvester: a purely resistive load and a full-wave rectifier before the load. A prototype capable of varying the amplitude and frequency of the input mechanical stimulus was constructed in order to evaluate the energy harvester. Then system identification techniques were employed to determine how the resonance frequency and output power are affected by the load. Experimental results showed that depending on the load there is significant change on the operating point at which the maximum power transfer occurs.

Keywords Energy harvesting · Frequency response · Output load · Piezoelectricity

1 Introduction

In recent years, the minimization of power consumption in electronic circuits competes with energy availability of harvesting sources. This concept is applied in many areas, from health and lifestyle equipment (Platt et al. 2005), energy supply in human body sensors to observe walking motion (Kuang et al. 2017), automobiles (Pan et al. 2017), intelligent buildings (Bao and Tang 2017), vibration monitoring for predictive maintenance in machinery (Das et al. 2017) and radio-frequency identification (Vullers et al. 2010).

Energy harvesting through piezoelectric transducers is based on the property of some materials that are capable to convert a mechanical stimulus into electrical energy. This kind of energy source has been employed in low power applications such as sensor nodes (Beeby et al. 2006; Du et al. 2017a), and microelectromechanical systems (MEMS) (Hu et al. 2010). In some of these applications, the integration of piezoelectric harvesters with other energy sources such as solar are also considered (Arms et al. 2005; Hsieh et al. 2016).

✉ M. A. J. Coelho
marcos.coelho@ufrgs.br

[1] Electrical Engineering Graduate Program, Federal University of Rio Grande do Sul, Porto Alegre, RS, Brazil

Piezoelectric energy harvester (PEH) generates electrical charge when mechanically strains occur in the material. As an intrinsic characteristic, the equivalent electric circuit of a piezoelectric material presents a capacitive response (Priya 2007; Liang and Liao 2011). Because the maximum power transfer is obtained when the load impedance matches with the PEH impedance (Alexander and Sadiku 2013), the knowledge of the load characteristics is required to increase the generation capacity of energy on the harvester output.

The mechanical stimulus needs to be dynamic in order to generate energy on the PEH. Thus, one can expect a variable generated voltage and a variation of equivalent impedance of the harvester. By considering a fixed purely resistive load, the maximum transferred power to the harvester output is dependent of the input mechanical frequency and will reach a maximum when the intrinsic impedance matches the load impedance. A prototype of impact-based PEH described by He et al. (2017) uses this concept for estimating the optimal impedance for generation at low frequencies.

The voltage waveform generated by PEH is time-varying and can be approximated by a sinusoidal function . However, because the majority of electronic equipments is powered by DC current a AC/DC converter with a full diode bridge (Naikwad et al. 2017) is usually connected at the output of the PEH, introducing a nonlinearity into the system. The search for generation efficiency involves mathematical modeling of AC/DC converter (Guan and Liao 2007; D'hulst and

Driesen 2008). Again, the process to optimize the transfer of generated power is matching the impedance between the PEH and the nonlinear load (Brufau-Penella and Puig-Vidal 2009). In Shu and Lien (2006) results of a PEH connected to an AC/DC converter are reported. The generated power is analyzed, concluding that the harvested power depends on the input vibration characteristics (frequency and acceleration), the mass of the generator, the electrical load, the natural frequency, the mechanical damping ratio, and the electromechanical coupling coefficient of the system. The theoretical analysis demonstrates that, even with a nonlinear behavior, there is an optimum load for maximizing the power delivered to the load.

This paper presents the results of a PEH coupled to an aluminum cantilever beam. The mechanical stimulus is performed by an electromechanical transducer in order to allow frequency and amplitude control of the cantilever beam. The control is performed by a low power signal connected to the input of a power amplifier driving the electromechanical transducers. The piezoelectric energy harvester (PEH) patch is attached on the cantilever, at strategic position, and its output terminals are connected to different electrical loads.

Firstly, the paper presents the mathematical model of the system and their theoretical modal frequencies. The load values representing the maximum delivered power are identified at each natural resonance frequency by connecting resistive loads to the output. The same analysis is done to a nonlinear load, by using the equivalent impedance, composed by a full bridge diode. The voltage and current generated from PEH are measured to determine the load equivalent impedance, as well as the generated power and DC voltage. Both cases are analyzed and compared when the output varies over a limited range of resistive values, representing a generic load, powered by different mechanical stimulus.

2 Energy Harvest System

Figure 1 shows the energy flow in a vibration-based generation system, where the source of vibration is coupled to the PEH. In the mechanical domain, the energy obtained from the source of vibration is partially converted into deformation, and partially dissipated in the form of heat (mechanical dissipation). After the conversion to electrical energy by the PEH, three effects can be noted regarding resulting energy: part is dissipated as heat (electrical dissipation); part returns to the mechanical domain due to the dual characteristic of the PEH; the remainder corresponds to the harvested energy effectively delivered to the load. In this context, the load value and characteristics alters the relation between the branches, i.e., altering the produced power and the mechanical characteristics of the energy harvester (Liang and Liao 2011).

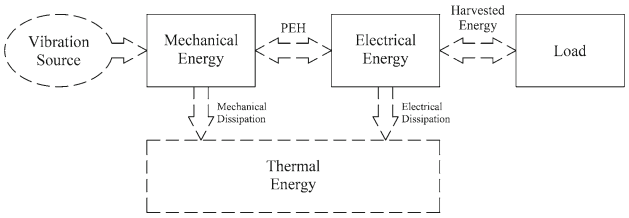

Fig. 1 Energy flow chart of a vibration energy harvester system

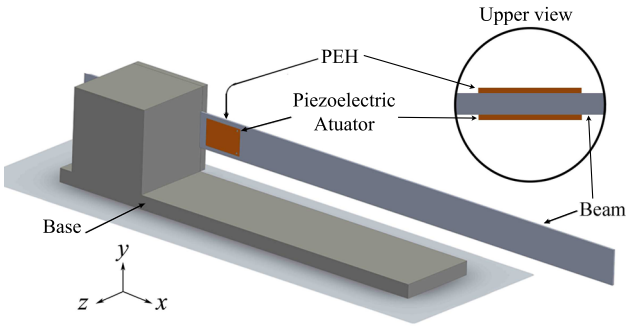

Fig. 2 Structure used for piezoelectric energy harvester

In this work, the effects of the output load in both electrical and mechanical domains will be analyzed with respect to the energy harvester illustrated in Fig. 2. A piezoelectric actuator attached to a aluminum beam and driven by a controlled oscillator is used as vibration source, where it is possible to regulate both amplitude and frequency. Our mechanical system consists of a flexible beam clamped to a fixed base at one of its ends. Finally, the PEH is the piezoelectric harvester attached at the opposite side of the vibration stimulus driven by the piezoelectric actuator.

2.1 Mechanical Model

The input stimulus is the voltage applied to the piezoelectric actuator, and the output is the measured voltage produced by the PEH.

The cantilever beam with a coupled piezoelectric actuator can be modeled through Euler–Bernoulli equations as described in Halim and Moheimani (2001), Moheimani and Fleming (2006) and Luemchamloey and Kuntanapreeda (2014):

$$\mathrm{EI}\frac{\partial^4 z(x,t)}{\partial x^4} + \rho A \frac{\partial^2 z(x,t)}{\partial t^2} = \frac{\partial^2}{\partial x^2} M_\mathrm{p}(x,t) \tag{1}$$

where I is the moment of inertia of the beam, A is the cross-sectional area, $M_\mathrm{p}(x,t)$ is the moment generated by the piezoelectric actuator in the point x (in relation to the length L of the beam) at time t, $z(x,t)$ is the beam displacement at (x,t), ρ is the bulk density, and E is the beam Young's constant. The following boundary conditions are considered: no displacement and inclination on the clamp end and the

absence of the bending moment and shear stress on the free end (Moheimani et al. 2003; Rao 2011). A set of decoupled ordinary differential equations can be obtained from (1) using the properties of the Dirac delta function and orthogonality. Thus, the differential equation of the beam/actuator system is described by Moheimani and Fleming (2006):

$$\frac{\mathrm{d}^2 r_i(t)}{\mathrm{d}t^2} + 2\zeta_i \omega_i \frac{\mathrm{d}r_i(t)}{\mathrm{d}t} + \omega_i^2 r_i(t) = \frac{\bar{k}}{\rho A}\psi_i V_\mathrm{a}(t) \tag{2}$$

where $i = 1, 2, \ldots$ is the vibration ith mode, ζ_i denotes the damping coefficient associated to this mode, ω_i is the natural oscillation frequency, $r_i(t)$ is the generalized coordinate of the ith mode of vibration, and ψ_i is the function dependent on the piezoelectric actuator relative position (Moheimani et al. 2003).

The frequency response that relates the piezoelectric transducer voltage $V_\mathrm{p}(i\omega)$ with respect to the controlled piezoelectric actuator (driving the mechanical stimulus) voltage $V_\mathrm{a}(j\omega)$ can be obtained from (2) and is given by Henrion et al. (2004):

$$\bar{G}_\mathrm{v}(j\omega) = \frac{V_\mathrm{p}(j\omega)}{V_\mathrm{a}(j\omega)} = P_\mathrm{v} \sum_{i=1}^{\infty} \frac{\Psi_i \Psi_i^T}{(j\omega)^2 + 2\zeta_i \omega_i (j\omega) + \omega_i^2} \tag{3}$$

where Ψ_i describes the actuator position and P_v is a constant depending on the beam structural properties. Note that (3) considers infinite vibration modes; nevertheless, it is well known from the literature that this relation can be approximated by assuming that the most of the output energy is concentrated in a finite number M of harmonic components as follows (Henrion et al. 2004; Moheimani and Fleming 2006):

$$G_\mathrm{v}(j\omega) = k_s \frac{\prod_{i=1}^{M} \left[(j\omega)^2 + 2\bar{\zeta}_i \bar{\omega}_i (j\omega) + \hat{\omega}_i^2\right]}{\prod_{i=1}^{M} \left[(j\omega)^2 + 2\zeta_i \omega_i (j\omega) + \omega_i^2\right]} \tag{4}$$

where k_s is a proportional gain derived from P_v, Ψ_i, ζ_i and ω_1. Parameters $\bar{\zeta}_i$ and $\bar{\omega}_i$ denote the natural oscillation frequency and damping coefficient associated with the zeros of the ith vibration mode.

2.2 PEH Equivalent Circuit

In the previous section, the frequency response of the cantilever beam was included in $G_\mathrm{v}(j\omega)$. Thus, the PEH stage can be modeled by an equivalent circuit composed of a series RC network with a voltage source for supplying the power to the circuit as illustrated in Fig. 3 (Priya 2007). Assuming that V_p is generated through the conditions described in the previous section, C_s and R_s denote the PEH internal capacitance and resistance, respectively, R_d is the dissipation resistance, and V_o represents the output voltage delivered to the load. The connection between this circuit and the load will be detailed in the next section.

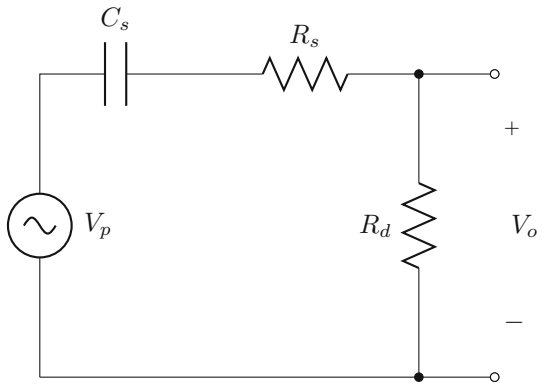

Fig. 3 PEH equivalent output circuit

2.3 Load

The PEH was subject to two different types of loads to evaluate its effects on the resonance frequencies and the output power: purely resistive load, composed of a single resistor and a full-wave rectifier in parallel with a RC load, characterizing a nonlinear load.

2.3.1 Purely Resistive Load

This case considers a purely resistive load R_L connected directly to the PEH equivalent circuit output V_o. From elementary circuit theory, it follows that the relation between the PEH voltage $V_\mathrm{p}(j\omega)$ and voltage delivered to the load $V_\mathrm{L}((j\omega)) = V_\mathrm{o}(j\omega)$ is given by:

$$G_\mathrm{L}(j\omega) = \frac{V_\mathrm{o}(j\omega)}{V_\mathrm{p}(j\omega)} = \frac{\frac{K_r}{(1+K_r)}(j\omega)}{(j\omega) + \frac{p_r}{(1+K_r)}},$$
$$K_r = \frac{R_\mathrm{d} R_\mathrm{L}}{R_\mathrm{s}(R_\mathrm{d} + R_\mathrm{L})}, \quad p_r = \frac{1}{R_\mathrm{s} C_\mathrm{s}}. \tag{5}$$

The equivalent circuit frequency response disregarding the output load can be derived from (5) assuming $R_\mathrm{L} \to \infty$.

2.3.2 Nonlinear Load

The inclusion of a full-wave rectifier introduces a nonlinear behavior at the equivalent circuit of the PEH, as presented in Fig. 4. In order to approximate the rectifier circuit by a linear load, the high-order harmonics in voltage signal are assumed to have insignificant contribution in output power

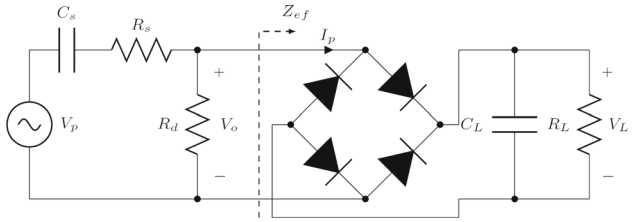

Fig. 4 Nonlinear load: full-wave rectifier connected to a load

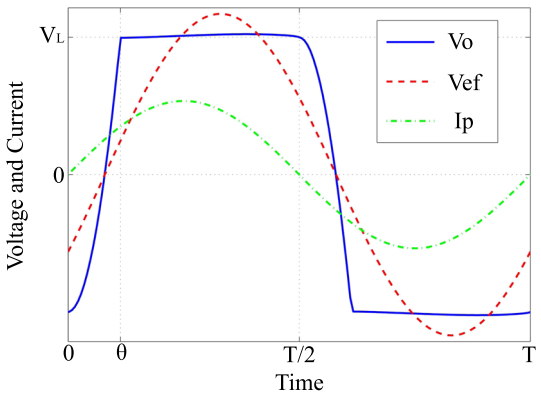

Fig. 5 Non-dimensional current, voltage and fundamental harmonic of the voltage in the PEH output connected to a full-wave rectifier

and only the fundamental harmonic has influence on the system dynamics (Liang and Liao 2012; Du et al. 2017b).

In this case, the PEH current can be approximated by a sinusoidal wave (Priya and Inman 2009). Figure 5 shows the non-dimensional characteristics of the current (I_p) and voltage (V_p) at the PEH output, with the voltage V_o being the value of the first harmonic of V_p. The rectifier nonlinear behavior is characterized by the constant voltage V_L (rectified voltage) after the cutoff angle (θ) that depends from load capacitance (C_L) and resistance (R_L). The rectified voltage V_L is the sum of voltage on capacitor C_L minus the voltage losses in the diodes.

The voltage $V_o(t)$ fundamental harmonic is given by (Liang and Liao 2012):

$$V_{ef}(t) = \frac{I_0}{2\pi\omega C_s}\{[sen(2\theta) - 2\theta]cos(\omega t) + 2sen^2(\theta)sen(\omega t)\} \quad (6)$$

where $V_{ef}(t)$ is the fundamental harmonic of $V_o(t)$, I_0 is current magnitude, and θ is the diode cutoff angle.

From (6), we obtain the equivalent impedance. Thus, only the fundamental component of the rectifier input $V_o(j\omega)$ is considered in such a way that the impedance of the load seen by the PEH patch (Z_{ef}) is the ratio between this voltage and PEH output current ($I_p(j\omega)$) (Liang and Liao 2012). Thus,

Table 1 Cantilever beam and piezoelectric propriety

Beam length, L (m)	0.71
Beam width, W (m)	0.05
Beam thickness, h (m)	0.003
Beam young's constant, E (N/m^2)	7×10^{10}
Beam bulk density, ρ (kg/m^3)	2770
Beam stand (kg)	30.11
Piezoelectric length, L_p (mm)	45.97
Piezoelectric width, W_p (mm)	33.27
Piezoelectric thickness, h_p (mm)	0.864

$V_o(j\omega) = V_{ef}(j\omega)$:

$$Z_{ef}(j\omega) = \frac{V_{ef}(j\omega)}{I_p(j\omega)} = \frac{1}{\pi\omega C_s}\left[sen^2(\theta) + j\,(sen(\theta)cos(\theta) - \theta)\right] \quad (7)$$

Assuming C_s constant, the impedance (Z_{ef}) depends only on ω and θ and is not dependent on the voltage source. The power delivered P_{ef} to the load Z_{ef} is described by (Liang and Liao 2012):

$$P_{ef} = \frac{1}{T}\int_0^T V_o(t)I_p(t)dt = \frac{1}{T}\int_0^T V_{ef}(t)I_p(t)dt \quad (8)$$

where T is the period in s.

3 Experimental Setup

In this section, the experimental setup is detailed and a complete frequency response is presented.

The cantilever beam constructive characteristics and the piezoelectric transducers' parameters are presented in Table 1, where the beam material was made from aluminum and both piezoelectric transducers were commercially available. More specifically, the piezoelectric actuator (used as mechanical stimulator) and harvester reference models are QP20W and V20W, respectively. These parameters are approximated and will be experimentally estimated through the system identification process to be described.

Figure 6 presents a descriptive block diagram of the experimental setup. A computer drives a real-time control board DS1104 in order to generate the input voltage to the piezoelectric transducer to mechanically stimulate the cantilever beam. The signal from the control board is conditioned by a low-pass filter with cutoff frequency of 400 Hz to attenuate any possible quantization noise. The frequency response of

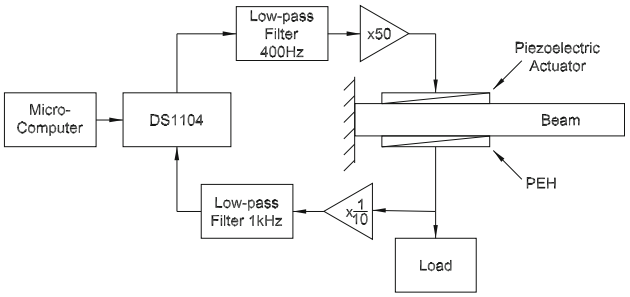

Fig. 6 Experimental diagram

this filter is given by:

$$G_{\mathrm{LP1}}(j\omega) = \frac{2\pi 400}{(j\omega) + 2\pi 400}. \tag{9}$$

In order to generate the maximum beam deformation, the filter output signal is amplified 50 times by a power amplifier (model QPA3202), assumed to be linear in the used frequency range, and connected to the electromechanical transducer. The piezoelectric harvester is attached to the cantilever beam and connected to the load, where the output voltage measurement is attenuated $10\times$ to adequate signal level. To avoid aliasing problems, this signal is filtered by a second-order filter with cutoff frequency of 1 kHz and frequency response given by:

$$G_{\mathrm{LP2}}(j\omega) = \frac{(2\pi 1000)^2}{(j\omega)^2 + (2\pi 1000)\sqrt{2}(j\omega) + (2\pi 1000)^2}. \tag{10}$$

In terms of signal propagation and frequency response, the experimental setup can be represented as in Fig. 7, where $\bar{V}_{\mathrm{a}}$ and $\bar{V}_{\mathrm{o}}$ denote the input and output signals of the dSpace card, respectively. By combining (4), (5), (9) and (10), it follows that the frequency response between $\bar{V}_{\mathrm{a}}$ and $\bar{V}_{\mathrm{o}}$ is given by:

$$\begin{aligned} G(j\omega) &= \frac{\bar{V}_{\mathrm{o}}(j\omega)}{\bar{V}_{\mathrm{a}}(j\omega)} \\ &= k_{\mathrm{amp}} k_{\mathrm{atn}} G_{\mathrm{v}}(j\omega) G_{\mathrm{L}}(j\omega) G_{\mathrm{LP1}}(j\omega) G_{\mathrm{LP2}}(j\omega) \end{aligned} \tag{11}$$

As described by (11), both $G_{\mathrm{v}}(j\omega)$ and $G_{\mathrm{L}}(j\omega)$ depend on constructive parameters and may vary with the load connected to the harvester output; hence, its precise characterization is not a trivial task. To determine these parameters as well as to take into account the tolerance in the nominal value of the components in k_{amp}, k_{atn}, $G_{\mathrm{LP1}}(j\omega)$ and $G_{\mathrm{LP2}}(j\omega)$, a system identification procedure is presented to determine $G(j\omega)$.

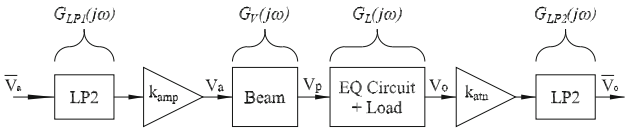

Fig. 7 The block diagram of the experimental setup in terms of signal propagation

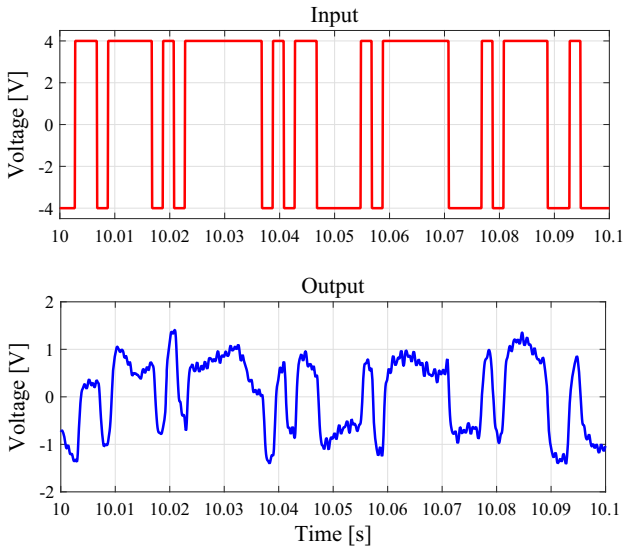

Fig. 8 PRBS input signal and the measured output signal

4 Results

Firstly the PEH frequency response is analyzed at open circuit. Thus, each load scenario is analyzed with respect to the measured output power.

4.1 System Identification at Open Circuit

The excitation signal, the number of poles and zeros of the desired model and the parameters and the optimization method should be defined in order to proceed with the system identification. In this work, a pseudorandom binary sequence (PRBS—persistently exciting signal in a given range of frequency) (Ljung 1999) ranging of ± 4 V with adjustable period was considered as input signal. Figure 8 illustrates the PRBS stimulus on the input piezoelectric transducer and from the PEH output measured signals.

Figure 9 shows the Power Spectral Density (PSD) function of signal measured on the PEH output from Fig. 8, where is possible to identify four ($M = 4$) natural vibration frequencies of $G_{\mathrm{v}}(j\omega)$. Because the low-pass filter with cutoff frequency at 400 Hz it follows that higher-order vibration modes are significantly attenuated and therefore can be neglected

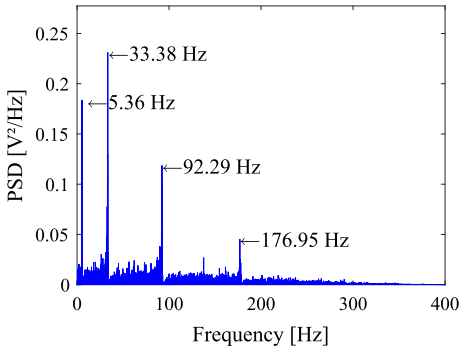

Fig. 9 PSD function of the output signal

The model to be identified corresponds to $G(j\omega)$ in (11) with $M = 4$, presenting nine zeros and twelve poles distributed as follows:

- a pair of complex zeros for each vibration mode;
- one zero derived from the equivalent circuit model;
- a pair of complex zeros for each vibration mode;
- one pole from the equivalent circuit model;
- three poles from the conditioning filters.

The system identification problem was solved in MATLAB with the system identification toolbox considering a continuous-time model, instrumental variables and nonlinear least squares as optimization method. The resulting transfer function (in the Laplace domain for simplicity) is

$$\begin{aligned} G(s) = & \frac{2.56 \times 10^3}{s + 2.56 \times 10^3} \times 50 \times \frac{1}{24.83} \\ & \times \frac{s^2 + 2 \times 0.0046 \times 35.06 s + 35.06^2}{s^2 + 2 \times 0.0045 \times 34.05 s + 34.05^2} \\ & \times \frac{s^2 + 2 \times 0.004 \times 214.25 s + 214.25^2}{s^2 + 2 \times 0.004 \times 209.23 s + 209.23^2} \\ & \times \frac{s^2 + 2 \times 0.0039 \times 588.23 s + 588.23^2}{s^2 + 2 \times 0.0040 \times 579.62 s + 579.62^2} \\ & \times \frac{s^2 + 2 \cdot 0.0042 \times 1125.82 s + 1125.82^2}{s^2 + 2 \times 0.0039 \times 1117.71 s + 1117.71^2} \\ & \times \frac{s}{s + 2598} \times 0.1 \times \frac{6597^2}{s^2 + 6597\sqrt{2} s + 6597^2} \end{aligned} \quad (12)$$

Figure 10 presents the frequency response magnitude of $G(s)$, where four vibration modes at frequencies $f_1 = 5.42\,\text{Hz}$, $f_2 = 33.38\,\text{Hz}$, $f_3 = 92.258\,\text{Hz}$ and $f_4 = 177.898\,\text{Hz}$ can be observed. We can also notice a zero at $\omega = 0$ and a pole at $f \approx 2.58\,\text{Hz}$ associated to the PEH equivalent circuit.

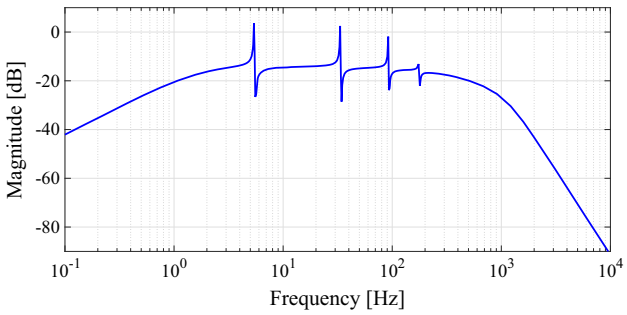

Fig. 10 Bode diagram of amplitude of theoretical and identified model

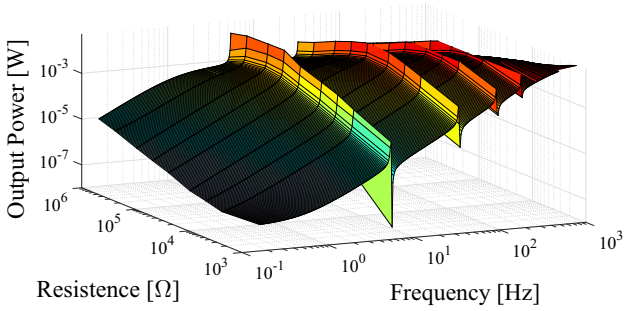

Fig. 11 Measured output power with resistive loads as function of frequency

4.2 PEH Output Power Analysis on a Connected Load

The piezoelectric harvester works with an intrinsic impedance. Thus, the power delivered to the load depends on the equivalent circuit from the terminals of the harvester device. One can expect that by changing the type of load, the power delivered also changes. We tested this hypothesis by using pure resistive load directly connected to the harvester terminals and by using the same resistive loads connected to a full-wave rectifier. A sine wave source with peak voltage in the range of $\pm 4\,\text{V}$ and a variable frequency of 0.1 Hz to 1 kHz was used to drive the piezoelectric transducer in order to mechanically stimulate the four identified modes of vibration.

Figure 11 shows the experimental results of the dependency of power delivered to resistances loads with respect to variation in the input frequency and load values. We observed that, as expected, the largest amplitudes of generation are concentrated in the natural vibration modes of the beam, where the mechanical deformation and the power generation of the PEH are high.

The PEH has an intrinsic capacitive impedance which directly influences the power delivered to the load. At low frequencies, the internal impedance of the PEH has a large value which falls with increasing the frequency ($X_c = 1/(j\omega C)$).

The instantaneous power values for purely resistive load as function of the natural vibration modes are shown in

Table 2 Instant power (mW) with resistive load as function the four natural vibration modes

Resistance (Ω)	1st mode	2nd mode	3rd mode	4th mode	Pulse
1 k	0.126	2.772	1.266	16.94	16.01
5 k	0.611	1.223	4.757	45.95	3.46
10 k	1.108	23.04	70.68	47.49	1.67
20 k	2.257	38.68	69.08	33.72	0.828
50 k	4.677	41.78	35.97	13.83	0.306
100 k	9.571	24.95	16.97	6.491	0.156
200 k	9.997	13.41	8.507	3.238	0.078
500 k	7.914	5.043	3.229	1.281	0.032
1 M	3.194	2.753	1.636	0.661	0.015

Table 2. The natural vibration modes correlate with the identified model in Sect. 4.1. Figure 10 is a slice of Fig. 11 with $R_L \to \infty$.

One can notice the highest power delivered to the purely resistive load is not obtained in the first mode of vibration (highest deformation) to resistors smaller than 200 kΩ. That occurs because of the intrinsic impedance of the piezoelectric harvester. The maximum power on the load occurs in the first mode of vibration to large resistors (500 kΩ and 1 MΩ), decreasing in higher vibration modes because these loads are much higher than the intrinsic impedance from the source. The highest power occurs to the load resistance of 200 kΩ for the first mode of vibration (5.42 Hz), close to the theoretical intrinsic impedance of the PEH (229.35 kΩ). The maximum power occurs to resistances of: 50 kΩ, 20 kΩ and 10 kΩ for the second, third and fourth modes, respectively. These results show that the source impedance decreases with increasing frequency.

In order to evaluate a transitory response of the system, a 22 ms voltage pulse was applied to the piezoelectric actuator, resulting a mechanical pulse excitation. The dependency of the generated RMS power to different load resistors is shown in the last column of Table 2. The maximum power transfer occurs at 1 kΩ resistance load. As the pulse signal has two distinct limits—rising and falling edge—where the power spectral presents high energy, the generated power at these points is much higher then the rest of the range. This happens because the PEH intrinsic capacitance presents low impedance at high frequencies. Thus, the optimum load resistance for generation tends to be the lowest because the internal impedance of the harvester is low.

The maximum power trend is shown in the contour plot of Fig. 12, of the measured power on the load. The arrow indicates the path of the maximum power as function of frequency and resistance. This trend depends on the harvester intrinsic impedance. The higher the excitation frequency of the system, the lower the impedance of the series capacitor. Therefore, the power transfer to the load (even the purely resistive load) is also dependent of the frequency. The instantaneous power generated at the vibration modes maintains this same behavior, as shown in Table 2.

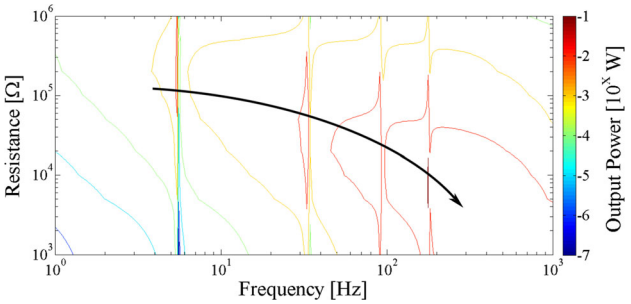

Fig. 12 Contour plot of output power with resistive loads as a function of frequency

Table 3 shows the equivalent impedance Z_{ef} (7) of the piezoelectric generator and the respective output powers when the PEH is connected to a full-wave rectifier before the load. Table 3 also shows that the equivalent impedance decreases with increasing the frequency.

By increasing the frequency, a large number of voltage/current cycles are rectified, also increasing the average voltage on the load. Table 3 also shows the voltage values on the load as a function of the load resistance and vibration modes. The voltage in the first mode of vibration is almost zero to 1 kΩ , raising to 5.82 V in the fourth mode. This behavior is followed by the loads of 10 and 100 kΩ. The load of 1 MΩ is much higher than the intrinsic impedance of the PEH, and the output voltage does not present significant change with different modes of vibration.

One can expect that the vibration frequency of the cantilever beam changes with the load. The observed change in resonant frequency of the vibration modes was about 0.2% (considering the experiment of only one PEH). This phenomenon occurs because the coupling factor k_{ij} and the elastic conformity coefficients of the piezoelectric element increase the mechanical rigidity, thus changing the equivalent electric circuit parameters. Although this effect is not significant with only one PEH, we can expect that with a

Table 3 Equivalent impedance Z_{ef}, output power P as function of frequency and resistance (mW) and continuous voltage in the load (V) (capacitor $C_L = 10\,\mu F$

Resistance (Ω)	1st mode			2nd mode			3rd mode			4th mode		
	Z_{ef}	P	V_{ref}	Z_{ef}	P	V_{ref}	Z_{ef}	P	V_{ref}	Z_{ef}	P	V_{ref}
1 k	1.808	0.001	0.03	1.707	0.204	0.452	1.623	0.568	0.754	1.528	0.636	0.798
10 k	9.328	0.041	0.64	7.817	1.661	4.075	5.953	2.943	5.425	4.420	2.073	4.553
100 k	63.25	0.237	4.87	27.31	2.544	15.95	12.24	1.814	13.47	6.725	0.752	8.673
1 M	98.56	0.161	12.68	36.07	0.505	22.47	13.35	0.261	16.15	6.950	0.089	9.452

large number of harvesters driving a load we will observe a larger change in the vibration frequency modes.

The presented results suggest that, in order to increase the power on a load, either after a rectifier (usual way) or directly connected to the PEH output we need to compensate the internal impedance from the harvesting device. This can be done by designing a PEH with a low intrinsic impedance or externally tune the impedance.

5 Conclusion

In this paper, we evaluated a piezoelectric energy harvester system directly connected to a resistive load and connected to a load through a rectifier circuit. Experimental results have showed that the insertion of the rectifier causes no significant change in the observations made on the purely resistive loads.

Also, the presented results showed that there is a dependency of the maximum power transfer with mechanical excitation frequency and load impedance. The maximum power transfer occurs when matching the intrinsic impedance of the piezoelectric energy harvester with the load. The intrinsic impedance of the piezoelectric harvester depends on the excitation frequency, and so the power transfer maximum to the load point.

As the results have shown, the parameters of equivalent circuit are dynamic, leading to the conclusion that the insertion of dynamic elements in the circuit can modify these parameters in order to increase power transfer, decreasing losses and increasing the efficiency of the system. This can be done, for instance by an external inductor in series with the load.

Acknowledgements We would like to thanks CAPES and FAPERGS for the research support - PqG 2110 − 2551/13 − 0. J.V. Flores was supported by CNPq (Brazil) under grants 43979/2014-6 and 305886/2015-0.

References

Alexander, C. K., & Sadiku, M. N. O. (2013). *Fundamentos de Circuitos Elétricos* (5th ed., p. 874). Porto Alegre: Bookman.

Arms, S., Townsend, C., Churchill, D., Galbreath, J., & Mundell, S. (2005). Power management for energy harvesting wireless sensors. In *SPIE international symposium on smart structures and smart materials* (Vol. 1, pp. 1–9).

Bao, B., & Tang, W. (2017). Semi-active vibration control featuring a self-sensing ssdv approach. *Measurement*, *104*, 192–203.

Beeby, S. P., Tudor, M. J., & White, N. M. (2006). Energy harvesting vibration sources for microsystems applications. *Measurement Science and Technology*, *17*(12), R175.

Brufau-Penella, J., & Puig-Vidal, M. (2009). Piezoelectric energy harvesting improvement with complex conjugate impedance matching. *Journal of Intelligent Material Systems and Structures*, *20*(5), 597–608.

Das, K., Zand, P., & Havinga, P. (2017). Industrial wireless monitoring with energy-harvesting devices. *IEEE Internet Computing*, *21*(1), 12–20.

D'hulst, R., & Driesen, J. (2008). Power processing circuits for vibration-based energy harvesters. In *IEEE power electronics specialists conference (PESC 2008)* (Vol. 39, pp. 2556–2562). New York: Rhodes.

Du, L., Fang, Z., Yan, J., & Zhao, Z. (2017a). Enabling a wind energy harvester based on ZnO thin film as the building skin. *Sensors and Actuators A: Physical*, *260*, 35–44.

Du, S., Jia, Y., & Seshia, A. A. (2017b). An efficient inductorless dynamically configured interface circuit for piezoelectric vibration energy harvesting. *IEEE Transactions on Power Electronics*, *32*(5), 3595–3609.

Guan, M. J., & Liao, W. H. (2007). On the efficiencies of piezoelectric energy harvesting circuits towards storage device voltages. *Smart Materials and Structures*, *16*(2), 498.

Halim, D., & Moheimani, S. O. R. (2001). Spatial resonant control of flexible structures—Application to a piezoelectric laminate beam. *IEEE Transactions on Control Systems Technology*, *1*(1), 37–53.

He, X., Teh, K. S., Li, S., Dong, L., & Jiang, S. (2017). Modeling and experimental verification of an impact-based piezoelectric vibration energy harvester with a rolling proof mass. *Sensors and Actuators A: Physical*, *259*, 171–179.

Henrion, D., Prieur, C., & Tliba, S. (2004). *Improving conditioning of polynomial pole placement problems with application to low-order controller design for a flexible beam* (Vol. 1, pp. 1–7). LAAS-CNRS Research Report 04163.

Hsieh, Y. T., Fang, C. L., Su, C. F., Tsai, H. H., & Juang, Y. Z. (2016). A hybrid ambient energy harvesting integrated chip (IC) for the internet of things (IoT) and portable applications. In *19th international conference on electrical machines and systems (ICEMS)* (pp. 1–4).

Hu, J., Jong, J., & Zhao, C. (2010). Vibration energy harvesting based on integrated piezoelectric components operating in different modes. *IEEE Transactions on Ultrasonics, Ferroelectrics, and Frequency Control*, *57*(2), 386–394.

Kuang, Y., Ruan, T., Chew, Z. J., & Zhu, M. (2017). Energy harvesting during human walking to power a wireless sensor node. *Sensors and Actuators A: Physical*, *254*, 69–77.

Liang, J., & Liao, W. H. (2011). Energy flow in piezoelectric energy harvesting systems. *Smart Materials and Structures*, *20*(1), 015,005.

Liang, J., & Liao, W. H. (2012). Impedance modeling and analysis for piezoelectric energy harvesting systems. *IEEE/ASME Transactions on Mechatronics*, *17*(6), 1145–1157.

Ljung, L. (1999). *System identification: Theory for the user* (2nd ed.). Upper Saddle River: Prentice Hall.

Luemchamloey, A., & Kuntanapreeda, S. (2014). Active vibration control of flexible beams based on infinite-dimensional Lyapunov stability theory: An experimental study. *Journal of Control, Automation and Electrical Systems*, *25*(6), 649–656.

Moheimani, S. O. R., Halim, D., & Fleming, A. J. (2003). *Spatial control of vibration: Theory and experiments, series on stability, vibration and control of systems* (Vol. 10, p. 223). Singapore: World Scientific.

Moheimani, S. R., & Fleming, A. J. (2006). *Piezoelectric transducers for vibration control and damping. Advances in industrial control* (1st ed.). London: Springer.

Naikwad, S., Rajendran, M. K., Sunil, P., & Dutta, A. (2017). A single inductor, single input dual output (sido) piezoelectric energy harvesting system. In *30th international conference on VLSI design and 2017 16th international conference on embedded systems (VLSID)* (pp. 95–100).

Pan, F., Xu, Z., Jin, L., Pan, P., & Gao, X. (2017). Designed simulation and experiment of a piezoelectric energy harvesting system based on vortex induced vibration. *IEEE Transactions on Industry Applications*, *99*, 1–1.

Platt, S., Farritor, S., & Haider, H. (2005). On low-frequency electric power generation with PZT ceramics. *IEEE/ASME Transactions on Mechatronics*, *10*(2), 240–252.

Priya, S. (2007). Advances in energy harvesting using low profile piezoelectric transducers. *Journal of Electroceramics*, *19*(1), 167–184.

Priya, S., & Inman, D. J. (2009). *Energy harvesting technologies*. Berlin: Springer.

Rao, S. S. (2011). *Mechanical vibrations* (5th ed., p. 1084). Upper Saddle River: Prentice Hall.

Shu, Y. C., & Lien, I. C. (2006). Analysis of power output for piezoelectric energy harvesting systems. *Smart Materials and Structures*, *15*(6), 1499.

Vullers, R. J. M., van Schaijk, R., Visser, H. J., Penders, J., & Hoof, C. V. (2010). Energy harvesting for autonomous wireless sensor networks. *IEEE Solid-State Circuits Magazine*, *2*(2), 29–38.